

pubs.acs.org/ac Article

# Insights into Spectral Distortion and Nonlinearity in UV—Vis and Fluorescence Spectroscopy of Molecular Fluorophore Solutions: Effects of Cascading Optical Processes (Part IV)

Pathum Wathudura, Joshua McEachin, and Dongmao Zhang\*



Cite This: Anal. Chem. 2024, 96, 13542–13550



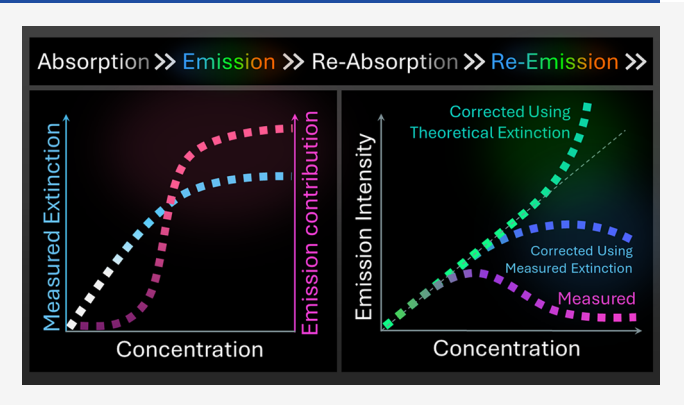
**ACCESS** I

III Metrics & More

Article Recommendations

S Supporting Information

ABSTRACT: Reproducibility and linearity are crucial benchmarks for any measurement technology. However, UV-vis and fluorescence spectral distortion and nonlinearity are prevalent, even in seemingly simple fluorescent solutions that comprise only one dissolved molecular fluorophore, without exogenous absorbing or scattering species. In this report, we introduce an analytical model for the quantification of fluorescence interference on UV-vis measurements and a conceptual model for mechanistically understanding the impacts of higher-order cascading optical processes on fluorescence measurements. The experimental UV-vis transmittance can be dominated by interfering fluorescence, even for fluorophore solutions with theoretical absorbance values far below the instrument's linear dynamic range (LDR).



Absorption-inner-filter-effect (aIFE) correction drastically improves the fluorescence LDR. However, the efficacy of aIFE correction hinges on two competing factors that strongly depend on the fluorophore's optical properties: the degree of fluorescence interference in UV—vis and the significance of secondary or higher-order emission triggered by fluorophore absorption of emitted photons. Our research sheds light on the remarkable complexity of cascading optical processes that can occur even in the simplest fluorescent solutions. It emphasizes the necessity of critically evaluating optical spectroscopic measurements of fluorescent solutions to improve the reliability of analyzing and interpreting optical spectra. Moreover, it lays the groundwork for future development of methods capable of handling challenging samples that exceed the capabilities of the current tools.

# INTRODUCTION

UV—vis and fluorescence are likely the most taught and applied measurement technologies serving various application objectives including chemical quantification, <sup>1,2</sup> materials characterization, <sup>3,4</sup> intermolecular interactions, <sup>5</sup> and intracellular imaging. <sup>6</sup> While UV—vis is generally viewed as a simple and robust measurement tool, spectral distortion and nonlinearity has been long documented for fluorescent solutions with theoretical absorbances within the instrument linear dynamic range (LDR). <sup>2,7–11</sup>

The analysis of fluorescence data presents an even greater challenge due to the intrinsic nonlinearity of fluorescence intensity  $I_{\rm F}(\lambda_{\rm x}\lambda_{\rm m})$  with respect to fluorophore concentration or absorbance  $A_{\rm x,f}$  at the excitation wavelength  $\lambda_{\rm x}$ , as described in the commonly used physical chemistry model (eq 1) for correlating fluorophore absorption and emission. The fluorescence quantum yield  $Q(\lambda_{\rm x}\lambda_{\rm m})$  is assumed to depend on both the excitation and detected emission wavelength  $\lambda_{\rm m}$ .  $I_0(\lambda_{\rm x})$  is the excitation intensity while  $R(\lambda_{\rm m})$  represents the detector responsivity

$$I_{\rm F}(\lambda_{\rm x}, \lambda_{\rm m}) = I_0(\lambda_{\rm x})R(\lambda_{\rm m})Q(\lambda_{\rm x}, \lambda_{\rm m})(1 - 10^{-A_{\rm x,f}}) \tag{1}$$

While eq 1 provides valuable photophysical insights into the origin of fluorescence, its practical utility in fluorescence measurements is limited, even for the simplest solutions containing only one type of molecular fluorophore with no exogenous light absorbers or scatterers. For example, eq 1 predicts that fluorescence increases monotonically with fluorophore concentration or UV—vis absorbance. However, the correlation between the experimental fluorescence and fluorophore concentration and absorbance is far more complex. It is a general observation that after a peak intensity is reached, fluorescence monotonically decreases with increasing fluorophore concentration. This is commonly referred to, in the literature, as the inner-filter effect (IFE). 7,8,11–15

Received: April 25, 2024 Revised: July 16, 2024 Accepted: July 20, 2024 Published: August 5, 2024





The validity of the theoretical model (eq 1) hinges on two critical conditions that are virtually impossible to meet in practical fluorescence measurements. First, it assumes that all emitted photons, regardless of their origination location and propagation directions, have an equal probability of being detected. Second, the model assumes that fluorescence involves only two cascading optical processes: photon absorption followed by fluorescence emission with no possibility of light absorption of the emitted photons. However, conventional spectrofluorometers detect only a portion of the fluorescence emission produced within the effective sampling volume defined by the pinhole effect of the instrument. Therefore, any absorption of excitation photons before they reach the effective sampling volume reduces the intensity of the excitation light within that volume, consequently decreasing the fluorescence intensity. This reduction in fluorescence caused by absorption of excitation photons is commonly referred to as the primary IFE in the literature. 7,14,15,18 We refer herein to the IFE due to absorption as (aIFE) to distinguish it from the IFE caused by light scattering, 19 as the scattering IFE behaves drastically differently than the aIFE.

Conversely, the absorption of emitted photons can occur whenever the fluoresced light falls within the wavelength region where the fluorophore absorption and emission spectra overlap. This results in reduced fluorescence intensity as well as spectral distortion because such signal attenuation depends strongly on the emission wavelength. The fluorescence spectral distortion and signal attenuation caused by the absorption of emitted photons is termed as secondary IFE in the literature, \$\frac{8}{12},18,20\$ or the secondary aIFE herein.

$$I_{\rm F}^{\rm corr}(\lambda_{\rm x},\,\lambda_{\rm m}) = I_{\rm F}^{\rm obsd}(\lambda_{\rm x},\,\lambda_{\rm m})10^{0.5A_{\rm x,f}+0.5A_{\rm m,f}} \eqno(2)$$

$$I_{\rm F}^{\rm corr}(\lambda_{\rm x},\,\lambda_{\rm m}) = I_{\rm F}^{\rm obsd}(\lambda_{\rm x},\,\lambda_{\rm m}) 10^{{\rm d}_{\rm x}A_{\rm x,f} + {\rm d}_{\rm m}A_{\rm m,f}} \eqno(3)$$

Since the 1950s, a plethora of research has been dedicated to improving the fluorescence linearity and correcting the spectral distortion caused by aIFE.  $^{10,12-14,16,18,20-33}$  Equation 2 shows the simplest and most used model for the correction of the aIFE in fluorescence spectra obtained with 1 cm  $\times$  1 cm square fluorescence cuvettes.  $I_{\rm F}^{\rm obsd}(\lambda_{\rm x}\lambda_{\rm m})$  and  $I_{\rm F}^{\rm corr}(\lambda_{\rm x}\lambda_{\rm m})$  are the asacquired and aIFE-corrected fluorescence intensities, respectively.  $^8$   $A_{\rm x,f}$  and  $A_{\rm m,f}$  are the fluorophore UV—vis absorbance values at excitation and emission wavelengths, respectively. This model assumes the spectrofluorometer including the cuvette is perfectly aligned, and the fluorescence excitation and detection are both aligned to the center of the cuvette. As such, the pathlength of the excitation and emission photons is 0.5 cm.

Equation 3 is a generalized model for aIFE correction where  $d_{\rm x}$  and  $d_{\rm m}$  are the effective excitation and emission pathlengths in fluorescence measurements, respectively. These pathlengths can be readily quantified by taking advantage of the aIFE on solvent Raman spectra. Consequentially, eq 3 enables aIFE correction regardless of the cuvette size and orientation.

Empirically, aIFE correction significantly enhances fluorescence spectral reproducibility and linearity. <sup>7,8,10,11</sup> For example, as-acquired fluorescence can deviate from linear dependence on fluorophore concentration even when its UV—vis absorbance at the excitation wavelength is as low as 0.05. <sup>9</sup> In contrast, aIFE-corrected fluorescence demonstrates a substantially higher upper limit for the linear dynamic range,

commonly assumed to be around 2. 12,15,34 However, beyond this extended upper limit, no existing IFE correction effectively rectifies the nonlinearity between the fluorescence intensity and fluorophore concentration.

To develop a mechanistic understanding regarding the effectiveness and limitation of aIFE correction in extending the fluorescence LDR, we proposed a first-principles model (eq 4) for correlating the experimental fluorescence with fluorophore light absorbance. 11 This model assumes that experimental fluorescence involves up to three cascading optical processes: fluorophore absorption of excitation photons, followed by emission, and subsequent absorption of the emitted photons. It is mathematically valid if the fluorophore UV-vis absorbance is less than 0.46 within the effective sampling pathlength or 1.4 for the fluorescence measured with our Fluoromax-4 spectrometer that has an effective sampling pathlength  $l_s$  of  $0.32.^{11} K(\lambda_x \lambda_m)$  represents the collective contribution of the instrument throughput for photons at the excitation and emission wavelengths, as well as the  $R(\lambda_m)$ . Detailed derivation of eq 4 is presented in an earlier publication.

$$I_{F}^{\text{obsd}}(\lambda_{x}, \lambda_{m}) = I_{0}(\lambda_{x})K(\lambda_{x}, \lambda_{m})Q(\lambda_{x}, \lambda_{m})l_{s}A_{x,f}$$

$$10^{-(A_{x,f}d_{x}+A_{m,f}d_{m})}$$
(4)

$$I_{\rm F}^{\rm corr}(\lambda_{\rm x}, \lambda_{\rm m}) = I_0(\lambda_{\rm x})K(\lambda_{\rm x}, \lambda_{\rm m})l_{\rm s}Q(\lambda_{\rm x}, \lambda_{\rm m})A_{\rm x,f} \tag{5}$$

The combination of eqs 3 and 4 leads to eq 5. Since  $I_0(\lambda_x)$   $K(\lambda_x\lambda_m)l_sQ(\lambda_x\lambda_m)$  is a constant under the measurement conditions, this equation provides a justification as to why the aIFE-corrected fluorescence using eq 3 is linearly correlated with the fluorophore solutions as long as the fluorophore absorbance at the excitation wavelength is less than 1.4. In practice, however, the upper LDR limit of the aIFE-corrected fluorescence varies significantly from fluorophore to fluorophore because of the fluorescence excitation and emission wavelengths.

The goal of this work is to derive a mechanistic understanding of the performance variety of the aIFE-correction method. Filling this knowledge gap is essential because aIFE correction has been commonly employed in analytical chemistry for identifying the factors responsible for fluorescence signal variations. For instance, concentration-dependent changes in fluorescence spectra can stem from various factors, including fluorophore aggregation, equilibrium between the same dissolved fluorophore in different structures or conformations, <sup>35–37</sup> or primarily from the complexities arising from the cascading optical processes inherent in the spectroscopic measurements of fluorescent solutions. Understanding the limitations of aIFE correction is important for enhancing the reliability of fluorescence data analysis.

This work is a continuation of our efforts to enhance evidence-based data interpretation of UV—vis and fluorescence measurements for optically complex solutions. We recently published a series of three articles on the effects of cascading optical processes, <sup>19,38,39</sup> the sequential photon/matter interactions triggered by the same incident photons, on spectroscopic measurements. Part I reported the impact of multiplicative scattering, the only cascading optical processes in scatterer-only solutions, on the UV—vis, scattering intensity, and scattering depolarization measurements. <sup>38</sup> Part II focused on the impact of cascading optical processes in solutions that contain both scatterers and absorbers but with no significant photoluminescence activities. <sup>39</sup> The cascading optical pro-

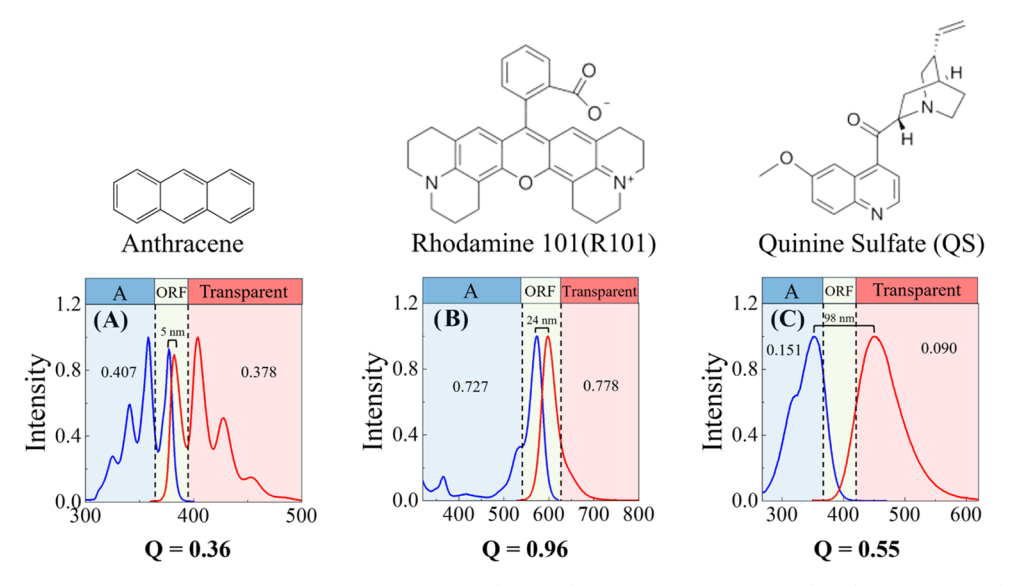


Figure 1. (Top) Structures and abbreviation of molecular fluorophores. (Bottom) Fluorescence excitation (blue) and emission (red) spectra of (A) anthracene, (B) R101, and (C) QS. The optical properties of fluorescent solutions under resonance excitation and detection conditions differ on the excitation wavelength. "A" refers to the wavelength region where the solution is approximately a pure absorber while ORF indicates the region where the fluorophore absorbs and emits at the same wavelength (on-resonance region). The region labeled "Transparent" indicates no significant photon/matter interactions at the specified wavelength region.

cesses in these solutions include multiplicative scattering and absorption of the scattered photons. The interplay among the light absorption and scattering complicates not only the experimental UV—vis extinction  $E_{\rm UV}(\lambda_{\rm x})$ , scattering intensity, and depolarization spectral analysis but also the experimental quantification of the actual number of photons absorbed even for solutions where the individual absorption and scattering extinction values are known. Part III, the final part of the serial publication, focuses on the impacts of the cascading optical processes on spectroscopic measurements of fluorescent solutions. However, with the only exception of UV—vis spectroscopic measurements, the studies of the fluorescent solutions are performed with fluorophore absorbance and nanoparticle scattering extinction of 1 or below.

The current study focuses on concentrated fluorescent solutions (up to ~1 mM) with theoretical UV-vis absorbance  $E_{\rm T}(\lambda_{\rm x})$  at excitation wavelengths reaching as high as 10. Model molecular fluorophores used in this study include anthracene, rhodamine 101 (R101), and quinine sulfate (QS) (Figure 1). These selections were made with two specific considerations in mind. First, their excellent solubility in their respective solvents ensures that the fluorophores are fully dissolved without significant aggregation. Therefore, the concentration-dependent spectral distortions or nonlinearity can be attributed to cascading optical processes or potential instrument issues, rather than changes in the fluorophore's physicochemical structures. Second, these model fluorophores exhibit distinct optical characteristics, as illustrated in Figure 1 and summarized in Table 1. These differences encompass variations in quantum yields and Stokes shifts as well as fractional absorption and emission within the on-resonancefluorescence (ORF)-active wavelength region compared to their absorption and emission spectra, respectively (Table 1). ORF refers to the fluorescence emission at the wavelength identical to the excitation photon wavelength. 40 ORF occurs where fluorophore's excitation and emission spectra overlap (Figure 1A–C).

Table 1. Integrated Quantum Yields Q, Fractional Absorption in the ORF Region, Fractional Emission in the ORF Region, and Stokes Shift of Anthracene, R101, and QS

	anthracene	R101	QS
Q	$0.36^{41}$	$0.96^{42}$	$0.55^{43}$
fractional absorption in the ORF region <sup>a</sup>	0.407	0.727	0.151
fractional emission in the ORF region <sup>a</sup>	0.378	0.778	0.090
Stokes shift (nm)	5	24	98

<sup>a</sup>Calculations for the fractional absorption/emission in the ORF region are shown in the Supporting Information.

# EXPERIMENTAL SECTION

Materials and Equipment. Analytical-grade anthracene (CAS: 120-12-7), Rhodamine 101 (R101) (CAS: 116450-56-7), toluene (CAS: 108-88-3), and sulfuric acid (CAS: 7664-93-9) were obtained from Sigma-Aldrich. Analytical-grade ethanol (CAS: 64-17-5) was purchased from Decon Laboratories, Inc. Analytical-grade quinine sulfate (QS) dihydrate (CAS: 6119-70-6) was purchased from Acros Organics. All chemicals were used as received without further purification. Nanopure water (18.2  $\rm M\Omega$  cm<sup>-1</sup>, Thermo Scientific) was used for sample preparation purposes.

An Evolution 300 UV-visible spectrophotometer (Thermo Scientific) was employed to acquire all UV-vis spectra, while fluorescence spectra were obtained using a Fluoromax-4 spectrophotometer (Horiba Jobin Yvon, Edison, NJ) equipped with excitation and detection linear polarizers.

**Sample Preparation.** Samples of anthracene, R101, and QS, each with varying concentrations, were prepared using toluene, ethanol, and 0.5 M sulfuric acid as solvents.

**Spectroscopic Measurements.** All spectrofluorometer-based spectra were acquired with an integration time of 0.3 s and a bandwidth of 2 nm for both excitation and detection monochromators. The spectral intensity for fluorescence measurements was reported as a ratio (S1/R1) between the signal from the sample detector (S1) and the reference detector (R1). All spectra were obtained using a  $1 \text{ cm} \times 1 \text{ cm}$ 

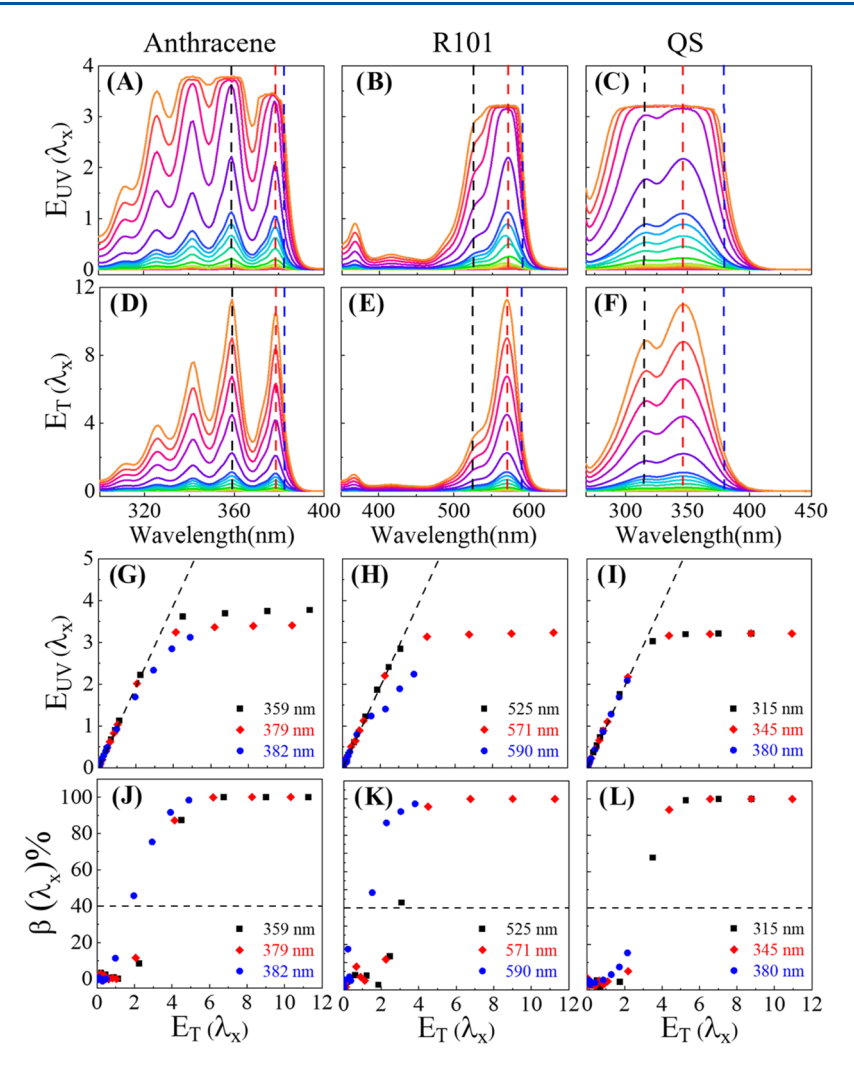


Figure 2. (A–C) Experimental UV–vis extinction, (D–F) theoretical UV–vis extinction, (G–I) experimental UV–vis as a function of the theoretical extinction, and (J–L) percentage fluorescence contribution to experimental UV–vis transmittance as a function of theoretical extinction for (A, D, G, J) anthracene, (B, E, H, K) R101, and (C, F, I, L) QS. The concentration range studied for each sample is 1  $\mu$ M to 0.89 mM, 0.1  $\mu$ M to 0.128 mM, and 2.0  $\mu$ M to 1.9 mM, respectively.

square Thorlabs fused quartz fluorescence cuvette with a sample volume of 3 mL at room temperature.

**LPAOS Acquisition.** Linearly polarized anti-Stokes-shifted, On-resonance, Stokes-shifted (LPAOS) spectroscopic acquisitions were performed by scanning from 50 nm below to 50 nm above the excitation wavelength. The excitation polarizer and detection polarizer were positioned vertically and horizontally (VH), respectively.

**Absorption-Inner-Filter-Effect Correction.** The absorption-inner-filter-effect correction of the as-acquired fluorescence spectra was conducted by utilizing eq 3. The  $d_{\rm x}$  and  $d_{\rm m}$  values employed in the equation were 0.44 and 0.55, respectively, quantified through the Solvent Raman method previously published.<sup>10</sup>

# ■ RESULTS AND DISCUSSION

**UV–Vis Spectroscopy.** The UV–vis spectrophotometer utilized in this study has an upper LDR limit of 5 in UV–vis absorbance, as specified by the vendor and experimentally verified in-house using KMnO<sub>4</sub> solutions. <sup>19,39</sup> When applied to fluorescent solutions, however, UV–vis spectra obtained with the same spectrophotometer exhibit significant spectral distortion and nonlinearity even when the sample experimental

UV—vis intensities all fall within the instrument LDR, and the spectra exhibit an excellent signal-to-noise ratio (Figure 2A—C). The solution's experimental UV—vis spectrum  $E_{\rm UV}(\lambda_{\rm x})$  is identical (within the measurement errors) to its counterpart theoretical UV—vis absorbance spectrum  $E_{\rm T}(\lambda_{\rm x})$  (Figure 2D—F) only when the fluorophore's UV—vis absorbance is below a certain threshold value. The  $E_{\rm T}(\lambda_{\rm x})$  spectra for the samples are determined using the molar absorptivity deduced from the Beer's-law-abiding experimental spectra acquired using diluted fluorescent solutions. <sup>19,38,39</sup>

While the instrument essentially has a wavelength-independent upper LDR limit of 5 for KMnO<sub>4</sub>, a molecular chromophore with no significant scattering and emission activities, <sup>19</sup> the upper UV—vis LDR limits for the molecular fluorophores are all significantly lower. For instance, the upper LDR limit extends to approximately 3 for QS, around 2 for anthracene, and as low as 1.5 for R101 at an excitation wavelength of 590 nm (Figure 2G–I). Further, the wavelength dependence of the upper UV—vis LDR limit differs significantly among these fluorophores. For instance, the LDR of QS is essentially independent of the excitation wavelength while that of anthracene and R101 is strongly wavelength-dependent. UV—vis spectra taken within their

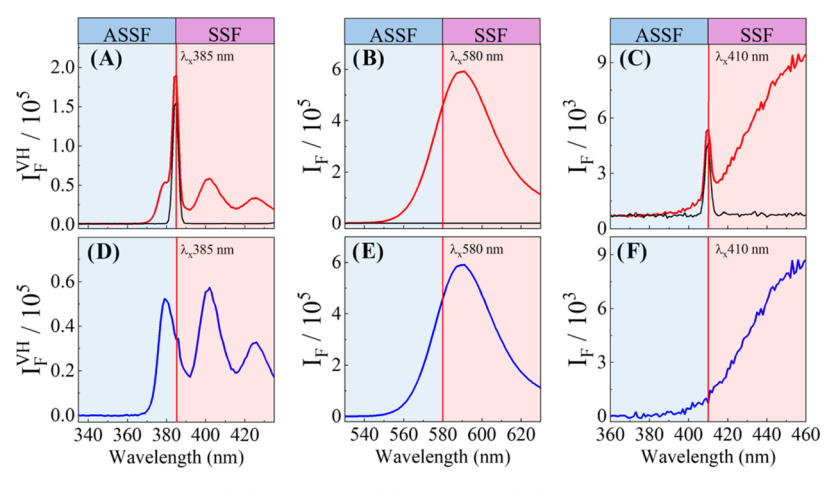


Figure 3. (Red) As-acquired LPAOS VH spectra of (A) anthracene, (B) R101, and (C) QS. The excitation wavelength is indicated with the middle red line. (Black) Solvent LPAOS spectra for identifying and subtracting the solvent light-scattering contribution to the fluorophore LPAOS spectra. (Blue) LPAOS fluorescence VH spectra of (D) anthracene, (E) R101, and (F) QS obtained through solvent spectral subtraction. ORF occurs at the excitation wavelength indicated with the dashed vertical line, when anti-Stokes-shifted fluorescence (ASSF) and Stokes-shifted fluorescence (SSF) are highlighted with blue and red, respectively.

ORF-active wavelength regions (labeled as ORF in Figure 1A,B) exhibit a lower upper LDR limit for both anthracene and R101. However, UV—vis spectra blue-shifted from their respective ORF-active regions (labeled as A in Figure 1A,B) show a consistently high upper LDR limit, close to 3, irrespective of the excitation wavelength for both fluorophores.

UV-vis can reliably quantify sample UV-vis extinction if the photons reaching the detector are predominantly intact incident photons.<sup>2,19,39</sup> For fluorescent and scattering solutions, however, it is inevitable that a small fraction of emission and scattered photons will reach the UV-vis detector. Such fluorescence and scattering interferences are negligible for diluted solutions but can be dominant contributors to the detected photons in concentrated lightscattering and/or light-emitting solutions.<sup>2,19</sup> Since the analytes used in this work have no significant scattering activities, the experimental UV-vis can be parametrized as eq 6.  $^{19,45}$   $F_{\rm UV}(\lambda_{\rm x})$  refers to the contribution of the fluorescence to the experimental UV-vis signal. The magnitude of  $F_{\rm UV}(\lambda_{\rm x})$  is heavily influenced by factors such as the instrument detection angle, detector responsivity to photons at various emission wavelengths, fluorophore quantum yield, and the intricate interplay between light absorption and emission, as elaborated in the Supporting Information.

$$E_{\text{UV}}(\lambda_{x}) = -\log \frac{I_{0}(\lambda_{x})10^{-E_{\text{T}}(\lambda_{x})} + F_{\text{UV}}(\lambda_{x})}{I_{0}(\lambda_{x})}$$
(6)

$$\frac{F_{\text{UV}}(\lambda_{x})}{I_{0}(\lambda_{x})10^{-E_{\text{UV}}(\lambda_{x})}} = 1 - 10^{(E_{\text{UV}}(\lambda_{x}) - E_{\text{T}}(\lambda_{x}))}$$
(7)

Rearranging eq 6 leads to eq 7, a mathematical model enabling experimental quantification of the fractional fluorescence contribution to the UV–vis transmittance  $\frac{F_{\rm UV}(\lambda_{\rm x})}{I_0(\lambda_{\rm x})10^{-E_{\rm UV}(\lambda_{\rm x})}}.$  For convenience, we define  $\beta(\lambda_{\rm x})\%=\frac{F_{\rm UV}(\lambda_{\rm x})}{I_0(\lambda_{\rm x})10^{-E_{\rm UV}(\lambda_{\rm x})}}\times 100$  as the percentage fluorescence contribution to UV–vis transmittance

PFCUT increases with increasing fluorophore concentration. Evidently, fluorescence interference is particularly

(PFCUT, pronounced as "P, F, CUT") (Figure 2J-L).

significant for anthracene and R101 UV—vis spectra. Even when the fluorophore  $E_{\rm T}(\lambda_{\rm x})$  is as low as 2, 40% of the detected photons in the UV—vis measurement can be due to fluorescence photons (Figure 2J,K). In contrast, a similar degree of fluorescence interference for QS appears only when the QS theoretical absorbance is  $\sim 3$  (Figure 2L).

Fluorescence-induced UV-vis spectral distortion and nonlinearity have been extensively documented in the literature.<sup>2,19</sup> This study provides an approach to quantify such fluorescence interference. However, attempts to devise a data analysis strategy for correcting these UV-vis abnormalities induced by fluorescence interference have proven challenging due to extraordinary complexity in the interplay among light absorption and emission. Figure 3 shows the LPAOS spectra of the fluorescent solutions excited at the wavelength where the UV-vis absorption and emission spectra shown in Figure 1 overlap. Qualitatively, the exceptionally high susceptibility of R101 and anthracene UV-vis intensities in their ORF-active wavelength region to fluorescence interference can be attributed to the notable anti-Stokes' switched fluorescence (ASSF) and ORF activity observed with excitation at the ORFactive wavelength. The fact that R101 UV-vis signal is most susceptible to fluorescence interference, followed by that of anthracene, is consistent with the fact that R101 has the strongest anti-Stokes-shifted fluorescence (ASSF) and ORF (Figure 3B,E), followed by that of anthracene (Figure 3A,D). In contrast, QS has negligible ASSF and ORF (Figure 3C,F). Critically, the ASSF and ORF photons can all be further absorbed and produce secondary emission, as will be discussed in the subsequent section.

Fluorescence Spectra. Fluorescence emission spectra were taken with the same set of fluorophore solutions used in Figure 2, where the theoretical UV—vis absorbance value of the most concentrated solution was as high as 10. The asacquired fluorescence emission and excitation spectra (Figures S1–S6) all exhibit nonlinearity and spectral distortion when the fluorophore absorbance at the excitation wavelength is above 0.1. The plots in the first and second columns of Figure 4 show only the subset of the as-acquired (Figure 4A,E,I) and aIFE-corrected (Figure 4B,F,J) spectra where spectral distortion and nonlinearity can be corrected by using

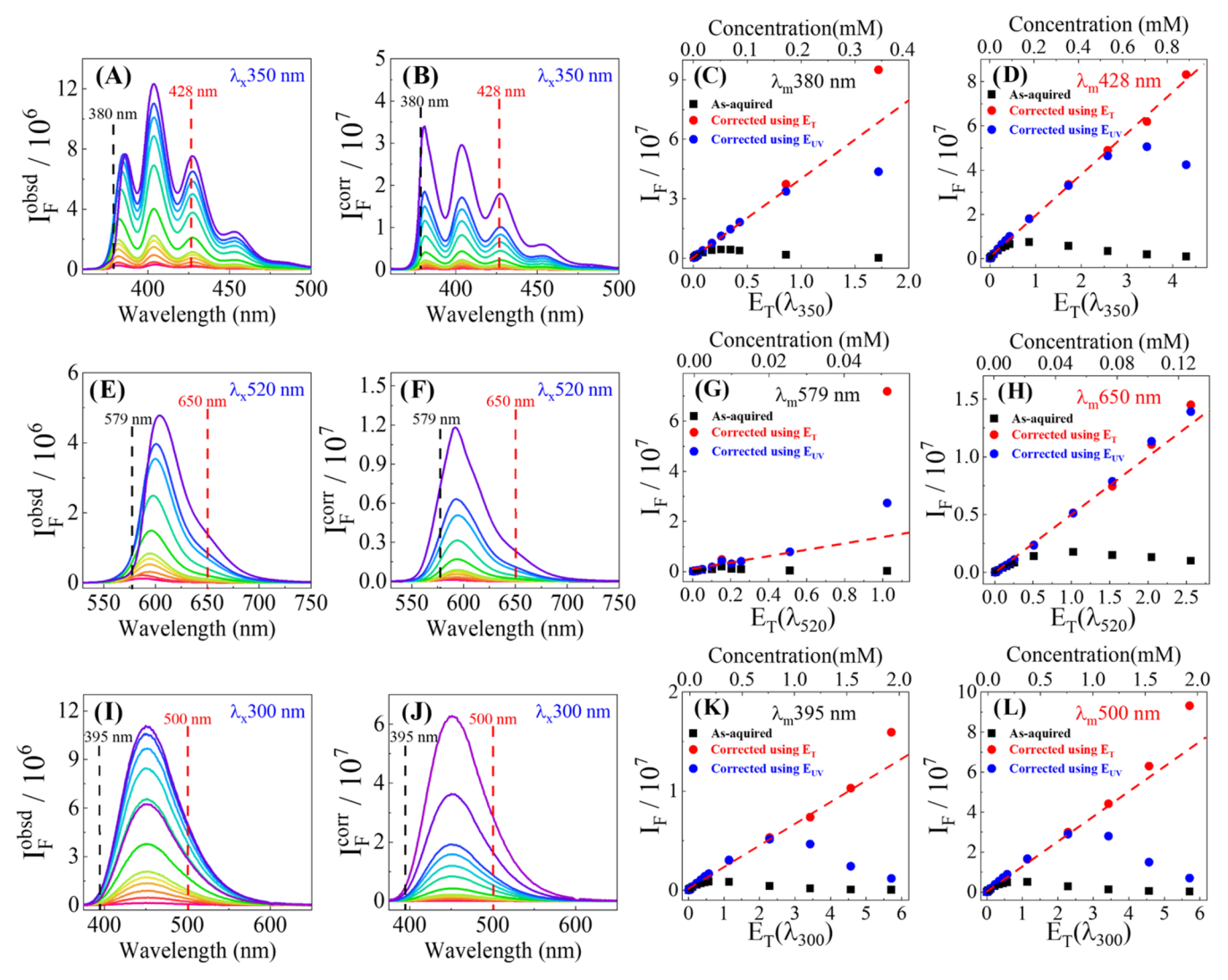


Figure 4. Fluorescence emission spectra of (top) anthracene, (middle) R101, and (bottom) QS. (A, E, I) As-acquired and (B, F, J) aIFE-corrected fluorescence emission spectra obtained using  $E_{\rm UV}(\lambda_{\rm x})$  for aIFE correction. These subset spectra are obtained with the low concentration solutions to show the threshold fluorophore absorbance, above which aIFE correction performed using  $E_{\rm UV}(\lambda_{\rm x})$  is ineffective. Complete sets of as-acquired and aIFE-corrected spectral data are presented in Figures S1, S3, and S5. (C, G, K) and (D, H, L) Correlations between the as-acquired, aIFE-corrected fluorescence, and the fluorophore concentration (upper x-axis) or  $E_{\rm T}(\lambda_{\rm x})$  (lower x-axis) at the fluorescence excitation wavelength. The emission wavelengths for the data in panels (C), (G), and (K) are in the fluorophore ORF-active region, while the emission wavelength for the data in panels (D), (H) and (L) are red-shifted from the ORF-active region.

experimental UV—vis  $E_{\rm UV}(\lambda_{\rm x})$  for aIFE correction (eq 3). The plots in the third and fourth column of Figure 4 compare the concentration dependence of the as-acquired and aIFE-corrected fluorescence intensities. The figures demonstrate the onset fluorophore concentrations or theoretical absorbance  $E_{\rm T}(\lambda_{\rm x})$  beyond which aIFE is grossly ineffective. The emission wavelength for Figure 4C,G,K is in the fluorophore ORF-active regions, while Figure 4D,H,L is red-shifted from the fluorophore ORF-active regions. A complete set of the data for all solutions used in Figure 4 is shown in Figures S1, S3, and S5.

The aIFE correction invariably improves fluorescence reproducibility and linearity, whether or not the experimental or theoretical UV—vis data are employed for the correction. However, there is no universal LDR for aIFE-corrected fluorescence. For example, upper LDR limits of the aIFE-corrected fluorescence in terms of fluorophore absorbance can be as low as  $\sim 0.5$  for R101 (Figure 4G) and as high as  $\sim 2.2$  for

QS (Figure 4K) when the fluorophore fluorescence is detected at their respective ORF-active region. Even for the same fluorophore, the upper LDR limit can also vary depending on the detection wavelength. For example, the upper LDR limit of the aIFE-corrected R101 fluorescence detected as its ORF-free wavelength 650 nm (Figure 4H) is  $\sim$ 2, approximately 4 times higher than that at the ORF-active region (Figure 4G).

For solutions that are too concentrated for effective aIFE correction, the experimental UV—vis leads to under-aIFE correction for anthracene (Figure 4C,D) and QS (Figure 4K,L) but overcorrection for R101 (Figure 4G,H). However, theoretical UV—vis absorbance  $E_{\rm T}(\lambda_{\rm x})$  invariably leads to overaIFE correction, i.e., the aIFE-corrected fluorescence intensities are higher than the linearly extrapolated intensities from the fluorescence data obtained with less concentrated solutions. The under-aIFE correction using the experimental UV—vis extinction can be explained by the fact that due to fluorescence interference, the experimental UV—vis extinction

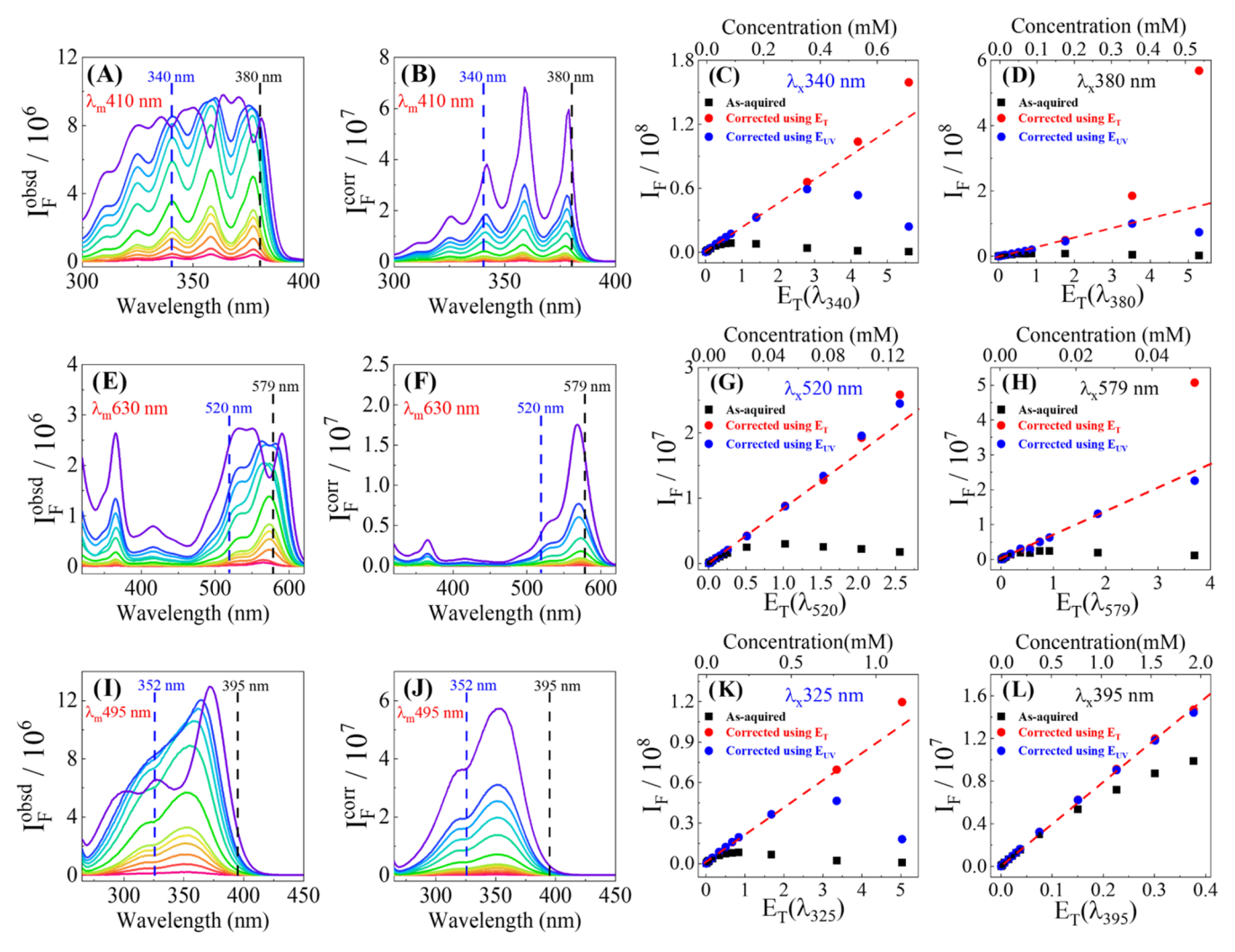


Figure 5. Fluorescence excitation spectra of anthracene (top row), R101 (middle row), and QS (bottom row). (A, E, I) As-acquired and (B, F, J) aIFE-corrected fluorescence excitation spectra obtained using  $E_{\rm UV}(\lambda_{\rm x})$  for aIFE correction. These subset spectra are obtained with the low concentration solutions to show the threshold fluorophore absorbance above which aIFE correction performed using  $E_{\rm UV}(\lambda_{\rm x})$  is ineffective. Complete sets of as-acquired and aIFE-corrected spectra are shown in Figures S2, S4, and S6. (C, G, K) and (D, H, L) Correlation between the as-acquired, aIFE-corrected fluorescence, and the fluorophore concentration (upper x-axis) or theoretical UV—vis absorbance  $E_{\rm T}(\lambda_{\rm x})$  (lower x-axis) at the fluorescence excitation wavelength. The excitation wavelengths for the data in panels (C, G, K) are blue-shifted from the fluorophore ORF wavelength region, while excitation wavelengths for the data in panels (D, H, L) are in the ORF-active region.

measurements underestimate fluorophore absorbance. The observation that even experimental UV—vis overcorrects R101 fluorescence and theoretical UV—vis overcorrects all fluorophore fluorescence suggests additional fluorescence emissions not accounted for by the aIFE correction model (eq 3) or by the first-principles model (eq 4). These models assume fluorescence involves only three cascading optical processes: absorption of the excitation light, emission, and reabsorption of the emitted light. However, the absorption of the emitted light can produce secondary emission, and so on.

$$I_{F}^{\text{obsd}}(\lambda_{x}, \lambda_{m}) = I_{0}(\lambda_{x})Q(\lambda_{x}, \lambda_{m})K(\lambda_{x}, \lambda_{m})l_{s}A_{x,f}$$

$$10^{-(A_{x,f}d_{x}+A_{m,f}d_{m})} + I_{F,HE}(\lambda_{x}, \lambda_{m})$$
(8)

$$\begin{split} I_{\text{F,SE}}(\lambda_{\text{x}}, \, \lambda_{\text{m}}) &= \int I_0(\lambda_{\text{x}}) Q(\lambda_{\text{x}}, \, \lambda_{\text{pm}}) K(\lambda_{\text{x}}, \, \lambda_{\text{m}}) l_{\text{s}} A_{\text{x,f}} \\ & 10^{-(A_{\text{x,f}} d_{\text{x}})} (1 \, - \, 10^{-A_{\text{pm,f}} d_{\text{m}}}) Q(\lambda_{\text{pm}}, \, \lambda_{\text{m}}) \, d\lambda_{\text{pm}} \end{split}$$

A revised model is developed herein (eq 8) to incorporate the contribution of fluorescence emission triggered by the absorption of any emitted photons to the experimental fluorescence, denoted as  $I_{\rm F,HE}(\lambda_{\rm x},\lambda_{\rm m})$  in eq 8. Unlike eq 4 that is an analytical model where all parameters are experimentally measurable or treated as constant, therefore directly applicable to model the experimental data, 11 eq 8 is a conceptual model for qualitative understanding of the impact of cascading light absorption and emission processes on the fluorescence signal. This model assumes that the aIFE within the effective sampling volume is negligible.

Deriving a mathematical expression for  $I_{\text{F,HE}}(\lambda_x \lambda_{\text{m}})$  is practically impossible. Even the model for the secondary emission intensity (eq 9) is mathematically intractable. The integral term in eq 9 describes the fact the secondary emission at the detected emission wavelength can be triggered by absorption of primary emission  $I_{\text{F,SE}}(\lambda_x \lambda_{\text{m}})$  as long as the primary emission wavelength  $\lambda_{\text{pm}}$  is within the fluorophore ORF-active region. A detailed derivation equation (eq 9) is shown in the Supporting Information.

$$I_{F}^{\text{corr}}(\lambda_{x}, \lambda_{m}) = I_{0}(\lambda_{x})Q(\lambda_{x}, \lambda_{m})K(\lambda_{x}, \lambda_{m})l_{s}A_{x,f}$$

$$+ I_{F,HE}(\lambda_{x}, \lambda_{m})10^{-(A_{x,f}d_{x} + A_{m,f}d_{m})}$$

$$(10)$$

Integrating the aIFE-correction model (eq 3) with the experimental fluorescence intensity model (eq 8) yields eq 10, highlighting that the effectiveness of the aIFE-correction method (eq 3) depends on two competing effects: the extent of fluorescence interference on fluorophore absorbance measurements and the magnitude of higher-order emission. While fluorescence interference leads to underestimated fluorophore absorbance, which results in under-aIFE-correction, higher-order emission leads to over-aIFE correction as mathematically expressed with the second term in eq 10. As a result, the upper LDR limit of the aIFE-corrected fluorescence is the fluorophore concentration below which both higherorder emission and fluorescence interference on UV-vis measurements are insignificant or the impacts of higher-order emission and fluorescence interference on UV-vis measurements on aIFE-correction compensate each other.

Using the theoretical UV-vis absorbance  $E_T(\lambda_x)$  for aIFE correction enables the determination of the threshold fluorescence concentration or absorbance beyond which higher-order emission is significant. Apparently, R101 has the lowest threshold absorbance, followed by anthracene and then QS. These results are consistent with the significance of the fluorophore absorbance and emission in its ORF-active wavelength region versus the entire fluorophore absorption and emission spectra (Figure 1). The fractional light absorption and emission values, in the ORF-active region, are 0.407 and 0.378 for anthracene, 0.727 and 0.778 for R101, and 0.151 and 0.090 for QS, respectively (Table 1). The lack of significant absorption and emission in the ORF-active region for QS explains why over-aIFE-correction occurs only when its theoretical absorbance  $E_{\rm T}(\lambda_{\rm x})$  at the excitation wavelength is as high as 5. In contrast, significant over-aIFE-correction appeared in R101 even when theoretical absorbance is as low as 1 (Figure 4G). Indeed, the higher-order emission in R101 is so high that even underestimated experimental UVvis can lead to over-aIFE-correction (Figure 4G,H).

Spectral distortion and nonlinearity are even more pronounced in fluorescence excitation spectra than in fluorescence emission spectra. Plots in the first and second columns of Figure 5 are the as-acquired (Figure 5A,E,I) and aIFE-corrected (Figure 5B,F,J) spectra, respectively. These spectra were acquired with the less concentrated fluorophore solutions for which the aIFE correction is effective to correct the spectral distortion and nonlinearity. These aIFE corrections are performed using the experimental UV-vis spectra (eq 3). A complete set of the data for all solutions used in Figure 5 is shown in Figures S2, S4, and S6. The third and fourth column plots in Figure 5 compare the concentration dependence of the as-acquired and aIFE-corrected fluorescence intensities (eq 3), which demonstrate the onset fluorophore concentrations or theoretical absorbance beyond which aIFE is grossly ineffective. The excitation wavelengths for Figure 5D,H,L are in the fluorophore ORF-active region while those for Figure 5C,G,K are blue-shifted from the fluorophore ORF-active regions.

The general observations on the effectiveness of aIFE correction from the fluorophore excitation spectra are consistent with those from the emission spectra. When aIFE correction is ineffective, the aIFE correction using fluorophore

theoretical UV—vis invariably causes over-aIFE-correction, while experimental UV—vis yields under-aIFE correction for anthracene and QS but overcorrection for R101. Overall, the upper LDR limits of the aIFE-corrected fluorescence depend on multiple factors including: (1) the experimental or theoretical UV—vis intensity used for the correction, (2) the excitation and emission wavelengths for the fluorescence measurements, and (3) the optical properties of the specific fluorophores including the fluorescence QY and the significance of fluorophore light absorption and emission in its ORF-active wavelength region.

# CONCLUSIONS

Cascading photon-matter interactions are intrinsic optical processes in the spectroscopic measurements of fluorescent solutions. Our study has revealed that these cascading optical processes can be highly complex even in the simplest fluorescent solutions comprising only dissolved molecular fluorophores, without any exogenous light absorbers or scatterers. The mathematical model we proposed for determining the percentage of fluorescence contribution to UV-vis transmittance provides a means for experimental quantification of fluorescence interference on UV-vis measurements. Remarkably, fluorescence interference can be substantial even when the fluorophore absorbance is as low as 1.5, well below the instrument LDR. In addition, we introduced an expanded analytical chemistry model for correlating fluorophore fluorescence and light absorption, which provides a mechanistic understanding of the effectiveness and limitation of aIFE correction for extending the fluorescence LDR. The upper LDR limit of aIFE-corrected fluorescence, in terms of fluorophore absorbance, is governed by two main factors: the accuracy of UV-vis measurements and the significance of higher-order emission. This limit ranges from smaller than 1 to larger than 3, depending on the optical properties of the fluorophore and the fluorescence excitation and detection wavelengths. Our work underscores the intricate nature of cascading optical processes even in seemingly simple fluorescent solutions that provide insights crucial for enhancing the reliability of data analysis and interpretation in UV-vis and fluorescence spectroscopy. Furthermore, our findings lay the groundwork for future investigations into the complexities of cascading optical processes in concentrated-nanoparticlecontaining fluorescent solutions, where scattering can further compound the complexity of spectroscopic analysis.

# ASSOCIATED CONTENT

### Supporting Information

The supporting information is available free of charge at https://pubs.acs.org/doi/10.1021/acs.analchem.4c02173.

Calculation of fractional absorption and emission in the ORF region; derivation of eq 6; parameterization of  $I_{F,UV}$  ( $\lambda_w \lambda_m$ ); derivation of eq 9; and complete emission and excitation spectra of anthracene, R101, and QS solutions (PDF)

# AUTHOR INFORMATION

# **Corresponding Author**

Dongmao Zhang — Department of Chemistry, Mississippi State University, Mississippi State, Mississippi 39762, United States; orcid.org/0000-0002-2303-7338; Phone: (662)-325-6752; Email: dongmao@chemistry.msstate.edu

#### **Authors**

Pathum Wathudura — Department of Chemistry, Mississippi State University, Mississippi State, Mississippi 39762, United States; © orcid.org/0000-0003-3846-812X

Joshua McEachin — Department of Chemistry, Mississippi State University, Mississippi State, Mississippi 39762, United States; © orcid.org/0009-0009-8280-8794

Complete contact information is available at: https://pubs.acs.org/10.1021/acs.analchem.4c02173

#### Notes

The authors declare no competing financial interest.

# ACKNOWLEDGMENTS

This work was supported in part by the Center of Biomedical Research Excellence Program funded through the Center for Research Capacity Building in the National Institute for General Medical Sciences (P20GM103646) and by an NSF Grant (CHE 2203571). The content is solely the responsibility of the authors and does not necessarily represent the official views of the National Institutes of Health or National Science Foundation.

# REFERENCES

- (1) Wu, P.; Hou, X.; Xu, J.-J.; Chen, H.-Y. Nanoscale 2016, 8 (16), 8427-8442.
- (2) Mäntele, W.; Deniz, E. Spectrochim. Acta, Part A 2017, 173, 965–968.
- (3) Zhong, F.; Zhao, J.; Hayvali, M.; Elmali, A.; Karatay, A. *Inorg. Chem.* **2019**, 58 (3), 1850–1861.
- (4) Davis, A. B.; Ihde, M. H.; Busenlehner, A. M.; Davis, D. L.; Mia, R.; Panella, J.; Fronczek, F. R.; Bonizzoni, M.; Wallace, K. J. *Inorg. Chem.* **2021**, *60* (18), 14238–14252.
- (5) Hu, M.; Sukhanov, A. A.; Zhang, X.; Elmali, A.; Zhao, J.; Ji, S.; Karatay, A.; Voronkova, V. K. J. Phys. Chem. B **2021**, 125 (16), 4187–4203.
- (6) Wang, Z.; Detomasi, T. C.; Chang, C. J. Chem. Sci. 2021, 12 (5), 1720–1729.
- (7) Kumar Panigrahi, S.; Mishra, A. K. J. Photochem. Photobiol., C 2019, 41, No. 100318.
- (8) Lakowicz, J. R. Principles of Fluorescence Spectroscopy; Springer, 2006.
- (9) Xu, J. X.; Vithanage, B. C.; Athukorale, S. A.; Zhang, D. *Analyst* **2018**, *143* (14), 3382–3389.
- (10) Nettles, C. B.; Hu, J.; Zhang, D. Anal. Chem. 2015, 87 (9), 4917-4924.
- (11) Wamsley, M.; Nawalage, S.; Hu, J.; Collier, W. E.; Zhang, D. Anal. Chem. **2022**, 94 (19), 7123–7131.
- (12) Holland, J. F.; Teets, R. E.; Kelly, P. M.; Timnick, A. Anal. Chem. 1977, 49 (6), 706–710.
- (13) Parker, C. A.; Rees, W. Analyst 1962, 87 (1031), 83-111.
- (14) Parker, C. A.; Barnes, W. Analyst 1957, 82 (978), 606-618.
- (15) Panigrahi, S. K.; Mishra, A. K. Photochem. Photobiol. Sci. 2019, 18 (2), 583-591.
- (16) Patra, D.; Mishra, A. K. Analyst 2000, 125 (8), 1383-1386.
- (17) Panigrahi, S. K.; Mishra, A. K. J. Phys. Chem. A 2019, 123 (50), 10815–10823.
- (18) Tucker, S. A.; Amszi, V. L.; Acree, W. E. J. Chem. Educ. 1992, 69 (1), No. A8.
- (19) Wamsley, M.; Wathudura, P.; Nawalage, S.; Zou, S.; Zhang, D. *Anal. Chem.* **2023**, 95 (27), 10279–10288.
- (20) Gauthier, T. D.; Shane, E. C.; Guerin, W. F.; Seitz, W. R.; Grant, C. L. *Environ. Sci. Technol.* **1986**, 20 (11), 1162–1166.
- (21) Puchalski, M. M.; Morra, M.; Von Wandruszka, R. Fresenius J. Anal. Chem. 1991, 340, 341–344.
- (22) Gu, Q.; Kenny, J. E. Anal. Chem. 2009, 81 (1), 420-426.

- (23) Kao, S.; Asanov, A. N.; Oldham, P. B. Instrum. Sci. Technol. 1998, 26 (4), 375-387.
- (24) Mode, V. A.; Sisson, D. Anal. Chem. 1974, 46 (2), 200-203.
- (25) Fanget, B.; Devos, O.; Draye, M. Anal. Chem. 2003, 75 (11), 2790–2795.
- (26) Luciani, X.; Mounier, S.; Redon, R.; Bois, A. Chemom. Intell. Lab. Syst. **2009**, 96 (2), 227–238.
- (27) Murphy, K. R.; Stedmon, C. A.; Graeber, D.; Bro, R. Anal. Methods 2013, 5 (23), 6557-6566.
- (28) Larsson, T.; Wedborg, M.; Turner, D. Anal. Chim. Acta 2007, 583 (2), 357-363.
- (29) Fonin, A. V.; Sulatskaya, A. I.; Kuznetsova, I. M.; Turoverov, K. K. PLoS One **2014**, 9 (7), No. e103878.
- (30) Sulatskaya, A. I.; Lavysh, A. V.; Maskevich, A. A.; Kuznetsova, I. M.; Turoverov, K. K. *Sci. Rep.* **2017**, *7* (1), No. 2146.
- (31) Credi, A.; Prodi, L. J. Mol. Struct. 2014, 1077, 30-39.
- (32) Andrade-Eiroa, A.; Vázquez-Blanco, E.; López-Mahía, P.; Muniategui-Lorenzo, S.; Prada-Rodríguez, D. *Analusis* **2000**, 28 (2), 148–154.
- (33) Kubista, M.; Sjöback, R.; Eriksson, S.; Albinsson, B. Analyst 1994, 119 (3), 417-419.
- (34) Wirth, M. J.; Lytle, F. Anal. Chem. 1977, 49 (13), 2054-2057.
- (35) Shustova, N. B.; McCarthy, B. D.; Dinca, M. J. Am. Chem. Soc. **2011**, 133 (50), 20126–20129.
- (36) Chan, F. T. S.; Schierle, G. S. K.; Kumita, J. R.; Bertoncini, C. W.; Dobson, C. M.; Kaminski, C. F. *Analyst* **2013**, *138* (7), 2156–2162.
- (37) Xu, S.; Liu, T.; Mu, Y.; Wang, Y. F.; Chi, Z.; Lo, C. C.; Liu, S.; Zhang, Y.; Lien, A.; Xu, J. Angew. Chem. 2015, 127 (3), 888–892.
- (38) Nawalage, S.; Wathudura, P.; Wang, A.; Wamsley, M.; Zou, S.; Zhang, D. Anal. Chem. 2023, 95 (3), 1899–1907.
- (39) Wathudura, P.; Wamsley, M.; Wang, A.; Chen, K.; Nawalage, S.; Wang, H.; Zou, S.; Zhang, D. *Anal. Chem.* **2023**, 95 (9), 4461–4469
- (40) Siriwardana, K.; Nettles, C. B.; Vithanage, B. C.; Zhou, Y.; Zou, S.; Zhang, D. Anal. Chem. **2016**, 88 (18), 9199–9206.
- (41) Berlman, I. Handbook of Florescence Spectra of Aromatic Molecules; Academic Press: New York, 1971.
- (42) Quintana Lazópulos, S.; Svarc, F.; Sagrera, G.; Dicelio, L. Cosmetics 2018, 5 (2), No. 33.
- (43) Eaton, D. F. Pure Appl. Chem. 1988, 60 (7), 1107-1114.
- (44) Zhang, W.; Zilevu, D.; Creutz, S. E.; Zhang, D. J. Phys. Chem. C **2020**, 124 (37), 20388–20397.
- (45) Wamsley, M.; Zou, S.; Zhang, D. Anal. Chem. 2023, 95 (48), 17426–17437.